SolarPACES 2023, 29th International Conference on Concentrating Solar Power, Thermal, and Chemical Energy Systems

Receivers and Heat Transfer Media and Transport: Point Focus Systems

https://doi.org/10.52825/solarpaces.v2i.834

Published: 15 Oct. 2024

Managing Heat Transfer Intensity in a Fluidized Particle-in-Tube Solar Receiver

Ronny Gueguen[1], Samuel Mer[2], Adrien Toutant[2], Françoise Bataille[2], and Gilles Flamant[1]

[1] PROMES-CNRS, Font Romeu, France

[2] PROMES-CNRS & UPVD, Perpignan, France

Abstract. Particle flow structure and associated heat transfer coefficient are examined as a function of temperature in a single-tube fluidized bed solar receiver operating in upward particle flow mode. It is found that temperature has a strong effect on both fluidization regimes and wall-to-bed heat transfer coefficient that varies in the range 800-1200 W/(m^2.K). Turbulent fluidization regime results in the most intense heat transfer between the irradiated wall and the fluidized particle.

Keywords: Particle-Driven CSP, Solar Receiver, Fluidized Bed, Heat Transfer

1. Introduction

In solar power tower, a heliostat field reflects the solar radiation toward a receiver located at the top of a tower, in which a HTF (Heat Transfer Fluid) circulates. At the outlet of the receiver, the hot HTF can be directly used to power a thermodynamic cycle, or stored to produce electricity on demand. In commercial towers, the commonly used HTF is molten salt, which has a working temperature ranging between 220 and 565 °C. In order to extend this range and, consequently, both increase the global plant efficiency and decrease its cost, several technologies using particles are currently developed at pilot scale [1]. The centrifugal receiver and the falling particle receiver are developed respectively by the DLR (Germany) [2] and Sandia (USA) [3]. Another concept of receiver is the particle-in-tube solar receiver, developed by CNRS – PROMES (France) [4]. In the latter, particles are fluidized and circulate upward in vertical metallic tubes. Particle temperatures at the outlet of the receiver up to 750 °C have been reached in earlier experiments [5], proving that highly efficient thermodynamic cycles can be used with this technology, for example sCO_2 cycles, hence improving the global plant efficiency. One of the main challenge of this concept is that several fluidization regimes can occur in the receiver tubes depending on the operation conditions [6]. Since these regimes govern the heat transfer properties, they strongly influence the receiver efficiency. Experiments have been conducted with a one-tube receiver at the 1 MW solar furnace (Odeillo, France) to characterize the hydrodynamics of the gas-particle flow and measure the associated heat transfer coefficients. This contribution summarizes the main results.

2. Experimental set-up

The experimental set-up is based on the single-tube solar receiver design described by [6] and presented in Figures 1a & b. Olivine particles of 61 µm mean diameter are fluidized in a vessel named “dispenser”, in which the receiver tube is immersed. The solar receiver made of Inconel,

is 3.20-meter high and 48-mm internal diameter. By applying an overpressure in the dispenser, particles circulate upward in the tube. A nozzle injects air at the bottom of the tube (called “aeration”) to stabilize the gas-particle suspension and control the fluidization regimes. Particles are heated over 1-meter long (between 0.6 and 1.6 m above the aeration) by concentrated solar power ranging between 220 and 600 Suns depending on the aiming strategy from the heliostats. Pressure probes and thermocouples are implemented in the set-up to determine the hydrodynamics of the particle flow in the tube. 196 batch tests have been performed during the experimental campaign in stationary conditions. The superficial air velocity in the tube varies between 0.03 and 0.47 m/s, the particle mass flux ranges from 0 to 93 kg/(m².s), and the corresponding particle temperatures are varying between the ambient and 700 °C. The variation of the air velocity in the injector enables controlling the fluidization regime in the tube. Consequently, the variation of the fluidization regime can be studied as a function of both air velocity and mean temperature in the irradiated zone.

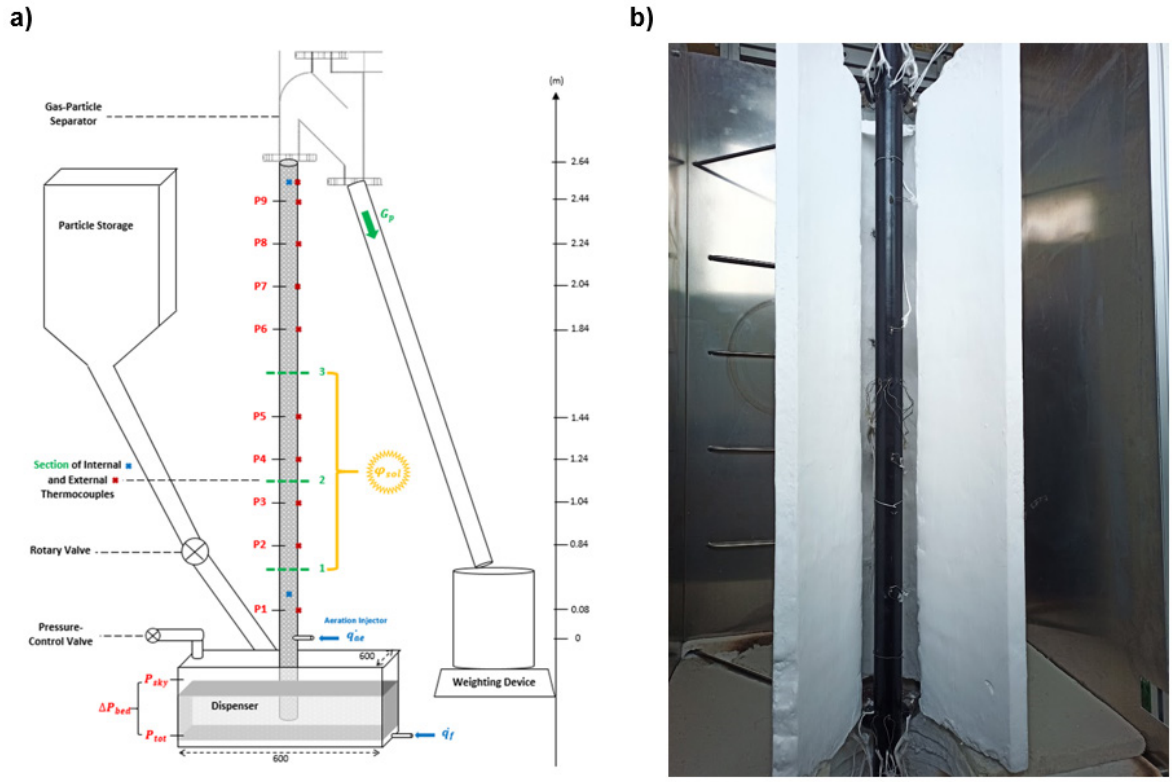

***Figure 1**. a) The experimental set-up and the associated instrumentation. In yellow, the irradiated section, and b) The absorber tube inserted in the solar receiver cavity.*

3. Experimental results

3.1 Fluidization regimes

Fluidization regimes are identified thanks to the combination of several analysis methods of the temporal pressure signals recorded at various heights in the receiver, detailed in [6]. Bubbling, wall slugging, axisymmetric slugging, turbulent fluidization and fast fluidization regimes have been identified. Their transitions are governed by the particle Reynolds number (Re_{slip}), calculated according to the local particle slip velocity ($U_{slip,i}$) with the following definitions:

$$U_{slip,i} = \frac{U_{air,i}}{1-\alpha_i} - \frac{G_p}{\rho_p \alpha_i} \quad (1)$$

$$Re_{slip} = \frac{\rho_{air} U_{slip} d_{SV}}{\mu_{air}} \quad (2)$$

Where α_i is the local particle volume fraction, G_p the particle mass flux, ρ_p and ρ_{air} the particle and the air density respectively, μ_{air} the air viscosity and d_{sv} the particle surface to volume mean diameter.

3.1.1. Fluidization regimes at ambient temperature

According to the previous methodology, the regime map plotted in Figure 2 was determined at ambient temperature. Bubbles are present at the bottom of the tube and coalesce with the height into axisymmetric slugs. The intermediate zone between bubbles and axisymmetric slugs is a coalescence zone, where wall slugs are present. At higher slip velocity, the interaction of the maximum bubble size wake with the following bubbles results in the splitting of the latter in small voids leading to the turbulent fluidization regime. At higher velocity, bubbles disappear and the gas solid flow structure is dominated by particle aggregates, the clusters, representative of the fast fluidization regime.

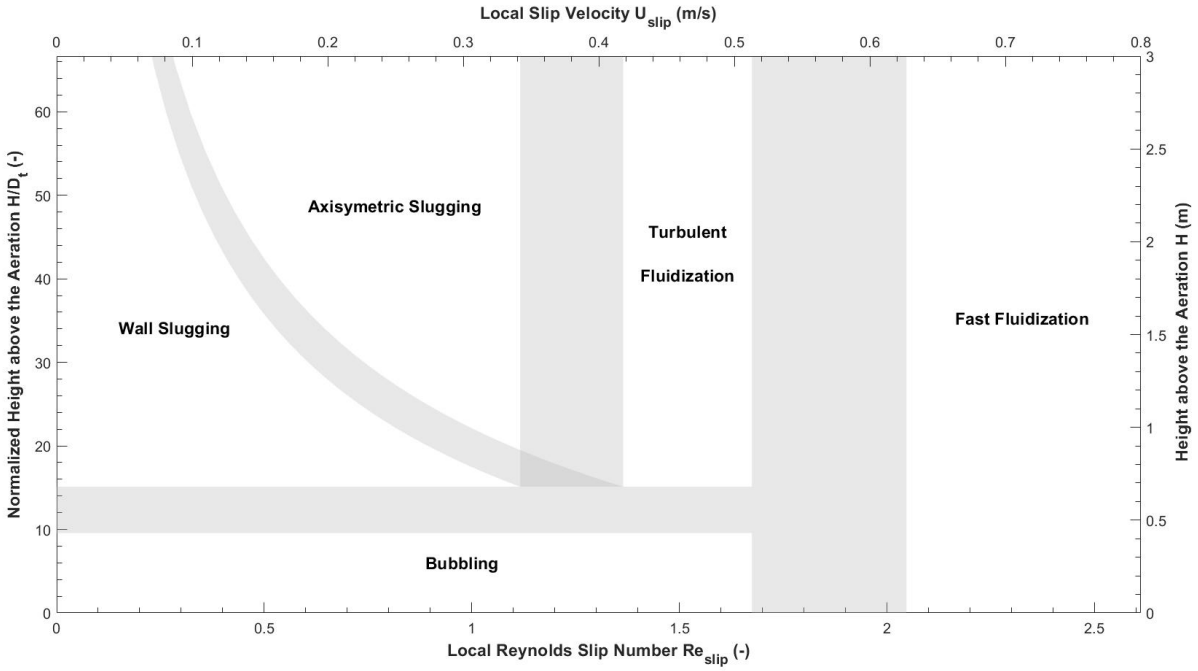

Figure 2. *Fluidization regimes determined in the solar receiver tube at ambient temperature, according to [6].*

3.1.2. Influence of temperature on the fluidization regime transitions

The effect of temperature on the fluidization regimes is detailed in [7]. Two transitions were particularly examined, the slugging to turbulent and the turbulent to fast fluidization regimes. Two main trends have been clearly identified. First, the transition limits (in terms of Re_{slip}) decrease with temperature. The values measured in the range 150-600°C are much lower than the transition limits determined at ambient temperature. For example, they are respectively 1.24 and 1.86 for the onset and the termination of the turbulent fluidization regime at ambient and approximately 0.3 and 0.2 at 500°C. Second, the size of the turbulent fluidization domain, i.e., the difference between the two transitions of regime, also decreases with temperature.

From the operation viewpoint, the main question to address is the effect of the fluidization regimes on the heat transfer intensity that govern the wall temperature for a given

incident solar flux and a targeted particle temperature. This key point is discussed in the next section.

3.2 Heat transfer coefficient

A global wall-to-particles heat transfer coefficient, $h_{wall,part}$ is calculated with Equations (3) and (4). This definition is similar to the classical formulation of convective exchange in a heat exchanger.

$$h_{wall,part} = \frac{\Phi_{abs}}{S_{exch}\Delta T_{wall,part}} \tag{3}$$

$$\Delta T_{wall,part} = \frac{\left(T^{in}_{wall,int} - T^{in}_{part}\right) - \left(T^{out}_{wall,int} - T^{out}_{part}\right)}{\ln\left(\frac{T^{in}_{wall,int} - T^{in}_{part}}{T^{out}_{wall,int} - T^{out}_{part}}\right)} \tag{4}$$

With $S_{exch} = \pi D_t H_{irr}/2$ (D_t the tube diameter and H_{irr} the irradiated height)and Φ_{abs} the power absorbed by the particles. The heat transfer coefficient as a function of the particle mass flux is plotted in Figure 3.

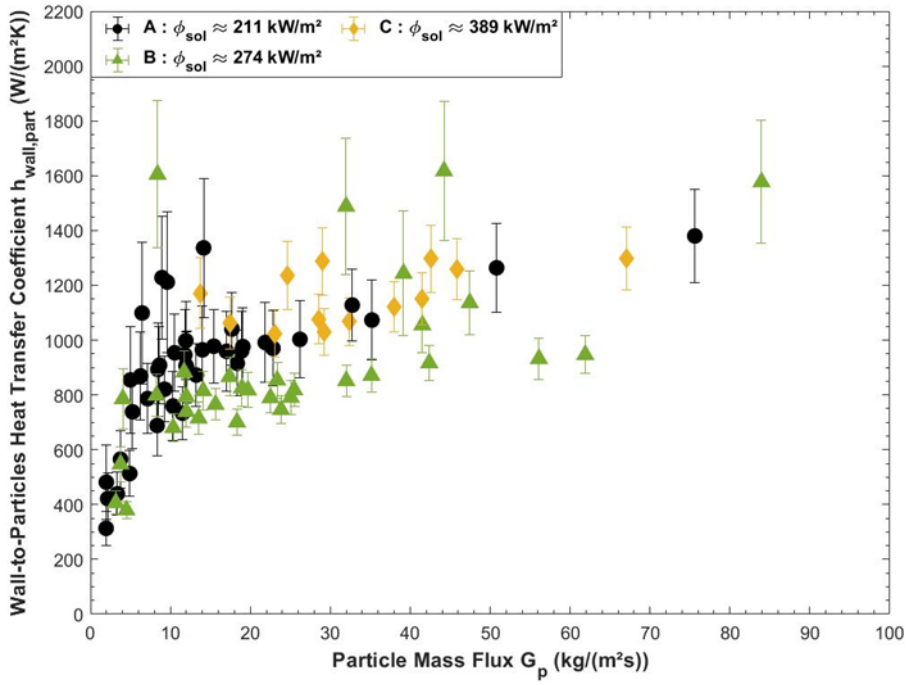

Figure 3. *The wall-to-fluidized bed heat transfer coefficient as a function of particle mass flux.*

Figure 3 indicates that for particle mass flux higher than 20 kg/(m^2.s) most of experimental data ranges between 800 and 1200 W/(m^2.K). Nevertheless, this representation does not give any indication on the influence of fluidization regime and temperature on the heat transfer intensity. In order to exhibit these effects, a non-dimensional index ($H_{wall,part}$) is introduced in Equation (5).

$$H_{wall,part} = \frac{h_{wall,part} S_{exch}}{G_p S_t C_{p,part}} = \frac{\Delta T_{part}}{\Delta T_{wall,part}} \tag{5}$$

This index is nothing but a Stanton number, which is classically used to assess the efficiency of heat transfer between a solid surface and a flow. Figure 4 illustrates the variation of $H_{wall,part}$ as a function of the slip Reynolds number with the fluidization regime as parameter. The

highest $H_{wall,part}$ is, the better the heat transfer since the same particle temperature increase is obtained for a lower temperature difference between the wall and the fluidized particles.

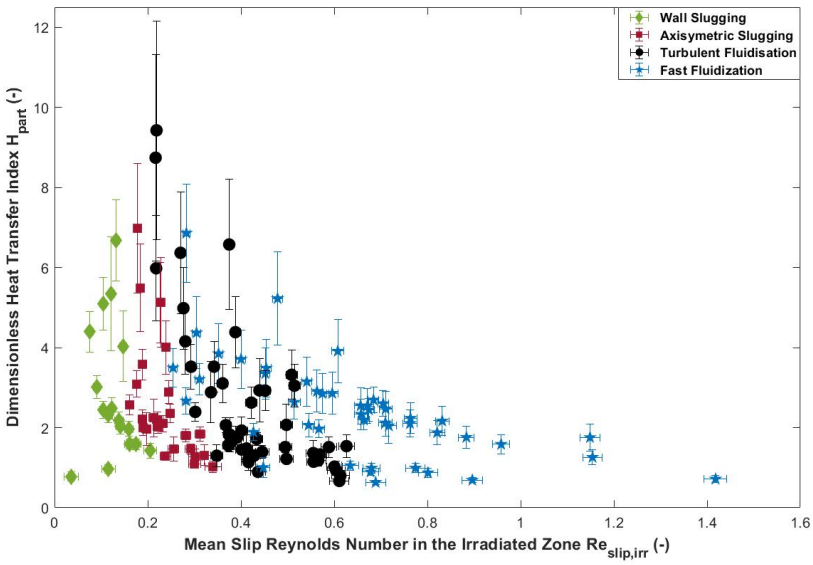

***Figure 4**. Heat transfer index as a function of the mean slip Reynolds number.*

Figure 4 shows clearly that for $Re_{slip,irr}$ in the range 0.2-0.4 the heat transfer intensity is the highest for the turbulent regime. For larger values the fast fluidization regime is preferable.

The effect of both fluidization regime and temperature is illustrated is Figure 5.

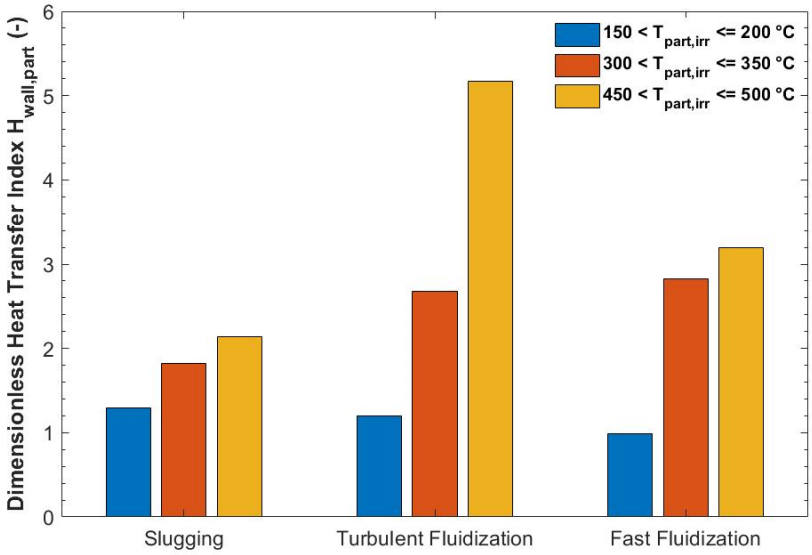

***Figure 5**. Heat transfer index as a function of fluidization regime and temperature.*

Figure 5 reveals three main results:

- At low temperature (<200°C), the heat transfer quality is similar for all the three regimes, slugging, turbulent and fast.
- At medium temperature (300-350°C), turbulent and fast fluidization reach the same level of heat transfer index.
- In the temperature range 450-500°C, turbulent fluidization exhibits by far the best heat transfer index.

4. Conclusion

The turbulent fluidization regime is associated to the best heat transfer. Actually, in this regime, the scission of the air structures is predominant compared to their coalescence that results in vortices and a strong particle mixing. The intermediate regime in terms of heat transfer is the fast fluidization, in which there is a phase inversion. There is a relatively dense zone at the bottom of the suspension followed by a dilute zone where clusters or particles are ejected upward [8]. Although the fast fluidization regime might be a good compromise for the heat transfer, it is more difficult to control the suspension from a practical point of view, and it needs high air velocities – i.e. high air flow rates – which is finally associated to high power consumption to compressed the air in the case of a commercial-scale power plant. Finally, the best compromise in terms of both heat transfer and energy consumption is the turbulent fluidization regime.

Data availability statement

Data can be assessed from direct query to the Authors.

Author contributions

Ronny Gueguen: Investigation, software, data curation, writing – review & editing, Samuel Mer: supervision, data curation, writing – review & editing, Adrien Toutant: supervision, validation, writing – review & editing, Françoise Bataille: supervision, data curation, writing – review & editing, Gilles Flamant: Conceptualization, funding acquisition, supervision, writing original draft.

Competing interests

The authors declare that they have no competing interests.

Funding

This work was funded by the French “Investments for the future” (“Investissements d’Avenir”) program managed by the National Agency for Research (ANR) under contract ANR-10-LABX-22-01 (Labex SOLSTICE).

Acknowledgement

Roger Garcia and Michael Tessonneaud are acknowledged for the experimental setup design and the assistance to experiments respectively.

References

1. G. Flamant, B. Grange, J. Wheeldon, F. Siros, B. Valentin, F. Bataille, , H. Zhang, Y. Deng, J. Baeyens. Opportunities and challenges in using particle circulation loops for concentrated solar power applications. Progress in Energy and Combustion Science 94, 101056, 2023. https://doi.org/10.1016/j.pecs.2022.101056.
2. W. Wu, L. Ambseck, R. Buck, R. Uhlig, R. Ritz-Paal, Proof of concept test of a centrifugal particle receiver, Energy Procedia, 49 (2014) 560-568. https://doi.org/10.1115/1.4030657.
3. C.K. Ho, G. Peacock, J. M. Christian, K. Albrecht, J. E. Yellowhair, and D. Ray. On-sun testing of a 1 MWt particle receiver with automated particle mass-flow and temperature

control. AIP Conference Proceedings 2126, 030027, 2019; https://doi.org/10.1063/1.5117539.

4. G. Flamant, D. Gauthier, H. Benoit, J.L. Sans, R. Garcia, B. Boissière, R. Ansart, M. Hemati, Dense suspension of solid particles as a new heat transfer fluid for concentrated solar thermal plants: On-sun proof of concept, Chemical Engineering Science, 102, 567-576, 2013. https://doi.org/10.1016/j.ces.2013.08.051.
5. H. Benoit, I. Pérez Lopez, D. Gauthier, J.L. Sans, G. Flamant, On-sun demonstration of a 750 °C heat transfer fluid for concentrating solar systems: Dense particle suspension in tube, Solar Energy, 118, 622-633, 2015. https://doi.org/10.1016/j.solener.2015.06.007.
6. R. Gueguen, G. Sahuquet, S. Mer, A. Toutant, F. Bataille and G. Flamant. Fluidization Regimes of Dense Suspensions of Group A Fluidized Particles in a High Aspect Ratio Column. Chemical Engineering Science, 267, 118360, 2023. https://doi.org/10.1016/j.ces.2022.118360.
7. R. Gueguen, S. Mer, A. Toutant, F. Bataille and G. Flamant. Effect of temperature on the hydrodynamics of a fluidized bed circulating in a long tube for a solar energy harvesting application. Chemical Engineering Science 281, 119218, 2023. https://doi.org/10.1016/j.ces.2023.119218.
8. Grace, J.R., Bi, X., Ellis, N. Chap. 9: Turbulent Fluidization, in: Essential of Fluidization Technology. John Wiley & Sons Ltd.: Chichester, U.K., pp. 163–180.